INT. J. NUM. METH. HEAT FLUID FLOW, VOL. 2, 79–86 (1992)

STABILITY OF NON-SIMILAR SHEAR LAYERS

M. G. MACARAEG

Theoretical Flow Physics Branch, MS156, NASA Langley Research Center, Hampton, VA 23665 USA

ABSTRACT

The present study is concerned with the stability and transition of a spatially evolving wake emanating from a splitter plate. Temporal linear stability calculations at different streamwise locations indicate significantly higher growth rates for mean flow profiles which occur near the trailing edge. Spatial simulations using these near wake mean flows exhibit non-linear roll-up for a case with Mach numbers of 2.76 and 1.87 on either side of the wake. If a similarity shear layer mean flow profile with these conditions is utilized in the simulation, no roll-up is obtained.

KEY WORDS Mach number Scramjet engine design Spatial simulations

INTRODUCTION

Supersonic combustion at high Mach numbers has become an important area of study for scramjet engine design. It is imperative that the shear layer between the two adjacent high-speed streams emanating from the scramjet be highly unstable so that fuel–air mixing is enhanced by turbulence. Past theoretical[1–3] and experimental studies[4] indicate a sharp drop off in mixing efficiency as Mach number is increased. Theoretical studies of shear layers have used simplified mean flows, such as hyperbolic tangent or similarity solutions. Chen *et al.*[5] studied the evolution of a temporally evolving wake assuming a Gaussian profile for the mean flow. The effect of Mach number and three dimensionality has been discussed via simulation and inviscid linear stability theory. Sandham and Reynolds[6] investigated the spatial evolution of an incompressible wake emanating off of a splitter plate, contrasting the physics of a forced versus unforced flow. Recent evidence[7] indicates that actual scramjet experiments do not suffer a great loss in mixing efficiency as Mach number increases[1–5]. The following study focuses on possible explanations of such discrepancies by considering the effect of Mach number on spatially evolving wakes.

MEAN FLOW PROFILES

The mean flows utilized in this study are solutions of the compressible boundary layer equations:

$$\frac{\partial}{\partial \bar{x}}(\overline{\rho u})+\frac{\partial}{\partial \bar{y}}(\overline{\rho v}=0 \tag{1a}$$

$$\overline{\rho u}\frac{\partial \bar{u}}{\partial \bar{x}}+\overline{\rho v}\frac{\partial \bar{u}}{\partial \bar{y}}=-\frac{\partial \bar{p}}{\partial \bar{x}}+\frac{\partial}{\partial \bar{y}}\left[\bar{\mu}\frac{\partial \bar{u}}{\partial \bar{y}}\right] \tag{1b}$$

$$\bar{\rho}\overline{Cp\tilde{u}}\frac{\partial \bar{T}}{\partial \bar{x}}+\bar{\rho}\overline{Cp\tilde{v}}\frac{\partial \bar{T}}{\partial \bar{y}}=\bar{u}\frac{\partial \bar{p}}{\partial \bar{x}}+\frac{\partial}{\partial \bar{y}}\left[\bar{\kappa}\frac{\partial \bar{T}}{\partial \bar{y}}\right]+\bar{\mu}\left(\frac{\partial \bar{u}}{\partial \bar{y}}\right)^2 \tag{1c}$$

$$\bar{p}=\bar{\rho}\bar{R}_g\bar{T} \tag{1d}$$

0961–5539/92/010079–08$2.00

Received April 1991
Revised September 1991

where $\bar{u}$ and $\bar{v}$ are the streamwise ($\bar{x}$) and normal ($\bar{y}$) velocity components, $\bar{T}$ the temperature, $\bar{p}$ pressure, $\bar{\rho}$ density, $\bar{\mu}$ viscosity, and $\bar{\kappa}$ conductivity. $\bar{R}_g$ is the universal gas constant. The flow is considered two dimensional. The specific heat at constant pressure, Cp, is assumed constant. Sutherland's law is assumed for viscosity, and conductivity is assumed to be proportional to viscosity.

Boundary conditions for the above system are given below:

$$\bar{u}(\bar{x},\infty)=\bar{u}_1; \qquad \bar{T}(\bar{x},\infty)=\bar{T}_1 \tag{1e}$$

$$\bar{u}(\bar{x},-\infty)=\bar{u}_2; \qquad \bar{T}(\bar{x},-\infty)=\bar{T}_2 \tag{1f}$$

where subscript 1 denotes the faster stream, and subscript 2 the slower stream. The final equations define an initial-boundary value problem. In the timelike (x) direction, straightforward use of fully-implicit, high-order backward finite-differencing is used to march the solution forward. In the normal direction, a spectral collocation method is employed. Details of this mean flow solution technique have been given[8] for a general curvilinear coordinate system and will not be repeated here. However, specific modification to this procedure necessary for the evolving wake solution are discussed below.

The initial condition is taken from similarity solutions[9] for compressible boundary layers. An approximation for the flow just after the trailing edge of the splitter plate is obtained by patching together two boundary layer profiles. It is assumed that the temperature at the plate for the 'fast side' $\bar{T}_{w1}$ is the average of the adiabatic wall temperatures for the two boundary layer flows as given below:

$$\frac{\bar{T}_{w1}}{\bar{T}_1}=0.5\left(\frac{\bar{T}_{aw1}}{\bar{T}_1}+\frac{T_{aw2}}{\bar{T}_2}\right) \tag{2a}$$

$\bar{T}_1$ and $\bar{T}_2$ are free stream temperatures, and $\bar{T}_{aw1}$ and $\bar{T}_{aw2}$ are the adiabatic temperatures of each side, respectively.

The normalized plate temperature on the 'slow side' is given by:

$$\frac{\bar{T}_{w2}}{\bar{T}_2}=\frac{\bar{T}_{w1}}{\bar{T}_1}\frac{\bar{T}_1}{\bar{T}_2} \tag{2b}$$

since $\bar{T}_{w1}=\bar{T}_{w2}$.

Flows are therefore considered non-adiabatic. The final equations are solved in non-dimensional form, where velocities and temperature are scaled by their free stream values and pressure is non-dimensionalized by $\bar{\rho}\bar{u}^2$. All lengths are scaled by a modified displacement thickness. Variables which follow are considered non-dimensional.

The mean flow profiles considered in the present study are taken sufficiently far from the splitter plate trailing edge so that the singularity in the boundary layer equation has no effect on the mean flow solution. It should be noted that the effect of this singularity is confined to a very small neighbourhood ($O(Re^{-3/8})$) of the trailing edge[10].

The evolving mean flow velocity profiles are compared with experimental profiles[11] in *Figure 1* for various downstream locations aft of the trailing edge. Conditions are chosen to match the experiments carried out by Demetriades[11], and are given in *Table 1*.

LINEAR STABILITY

Temporal linear stability analysis is performed at the streamwise locations depicted in *Figure 1*. Growth rates (ω_i) *versus* streamwise wavenumber α are given in *Figure 2*. Note the appearance of a higher mode at stations 1 and 6. This mode at higher α becomes weaker as the flow progresses downstream of the trailing edge. In addition, growth rates clearly decrease as the mean flow goes further downstream of the trailing edge (i.e., as a similar mixing layer profile is approached). Since the two inflection points of the wake profile render this flow more unstable than the

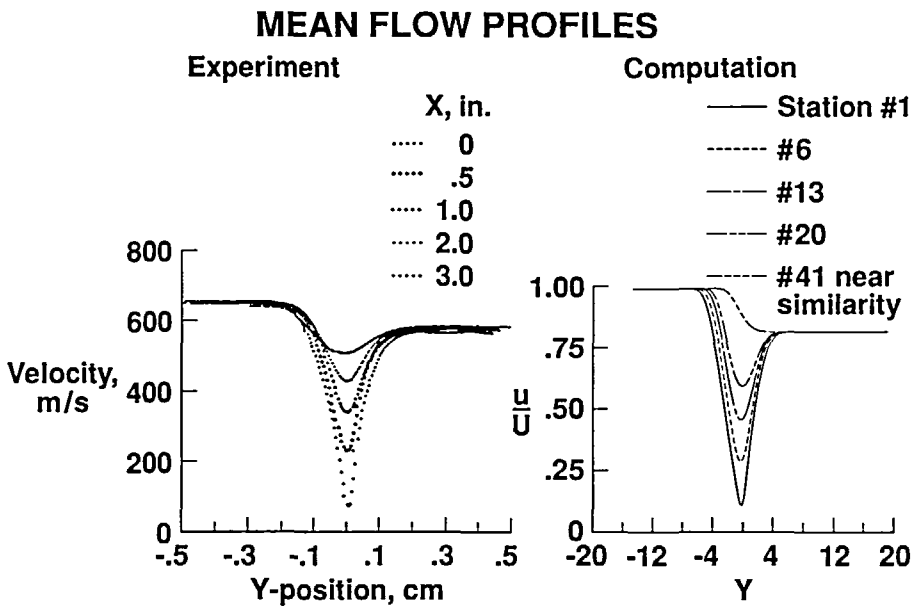

Figure 1 Mean flow velocity profiles of developing wake taken from experiment[11] and present computation. Case I: $M_1=2.76$, $M_2=1.87$, $T_\infty=127.7$K, $Re=50{,}000$, non-adiabatic

Table 1 Flow properties

Parameter	Case I	Case II
M_1	2.76	0.6
M_2	1.87	0.4065
U_2/U_1	0.8198	0.6775
$*T_{01}=T_{02}$(K)	322.2	322.2
T_1	127.7	287.7
T_2	189.6	298.0
$Re^{\delta**}$	50000	50000

* Stagnation temperature
** Reynolds number in terms of modified displacement thickness

dominant single inflection point of a mixing layer[12], these observations are not surprising. The station 41 profile is essentially that of a similarity free shear layer.

If we define a convective Mach number based on the phase speed of the maximally amplified disturbance[13] some interesting trends may be noted. The Mach numbers

$$M_{c1}=M_1\left(1-\frac{\omega_r}{\alpha}\right); \qquad M_{c2}=M_1\left(\frac{\omega_r}{\alpha}-\frac{\bar{u}_2}{\bar{u}_1}\right)\Big/\left(\frac{\bar{T}_2}{\bar{T}_1}\right)^{**0.5} \tag{3}$$

Are the convective Mach numbers with respect to the fast and slow stream, respectively. *Table 2* lists M_c for each station of *Figure 2*. Note that for profiles near the trailing edge the maximally-amplified mode has a phase speed less than the slower stream's velocity. The phase speed of the maximally-amplified disturbance increases as the profiles approach similarity.

The structural evolution of the unstable disturbance at station 1 is given in *Figure 3* for various streamwise wavenumbers. Depicted are the temperature, $\tilde{\tau}$, and normal velocity, $\tilde{v}$, disturbance

Table 2 Convective Mach numbers for case I: $U_2/U_1 = 0.8198$; $T_2/T_1 = 1.485$

Station	α_m*	ω_{max}	v_{ph}**	M_{c1}	M_{c2}
1	1.545	(1.167,0.2027)	0.7548	0.6768	−0.1472
6	1.625	(1.265,0.1857)	0.7783	0.6120	−0.09410
13	1.750	(1.427,0.1574)	0.8156	0.5088	−0.009423
20	1.711	(1.459,1229)	0.8527	0.4066	0.07452
41***	0.7669	(0.7982,0.02897)	1.0829	−0.08294	0.5960

* α corresponding to ω_{max}
** Phase speed
*** Nearly self similar

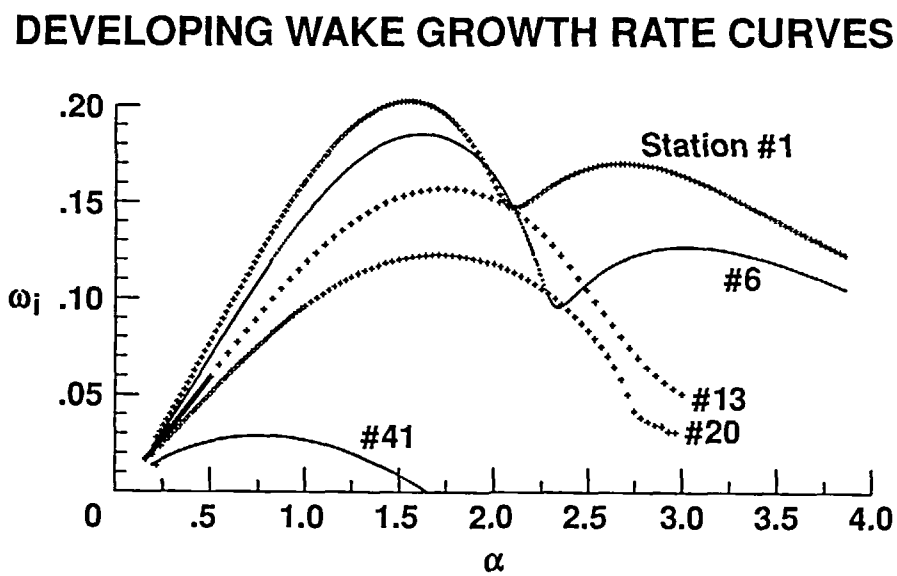

Figure 2 Temporal growth rates *versus* streamwise wavenumbers for computed mean flow profiles given in *Figure 1*

eigenfunctions. Note that as α increases the multiple lobe structure of the mode becomes more dominant.

For comparison, a second case is studied in which we retain the same Mach number ratio and stagnation temperature as the previous case. However, both streams are taken to be subsonic. These conditions are given in *Table 1*. Linear stability analysis at comparable streamwise locations as the previous case are performed. Growth rates versus α are given in *Figure 4* for stations 1, 13 and 41. For comparison, growth rates from the supersonic case are also given from *Figure 1*. No higher mode similar to Case I is seen for the subsonic case. As expected, the maximum growth rates are much higher for the lower Mach number case. However, it is found that the decrease in the growth rate with increasing Mach number is much smaller if mean flows near the trailing edge are compared. This difference is emphasized in *Figure 5*, which depicts growth rates versus α for the high and low Mach number case for station 13 and 41, respectively. Note that station 13 displays approximately a factor of two change in the maximum growth rate between the two cases, whereas, station 41 (nearly similar profile) displays a factor of four difference between the two cases. Clearly the effect of Mach number is greater for the nearly similar mean flows.

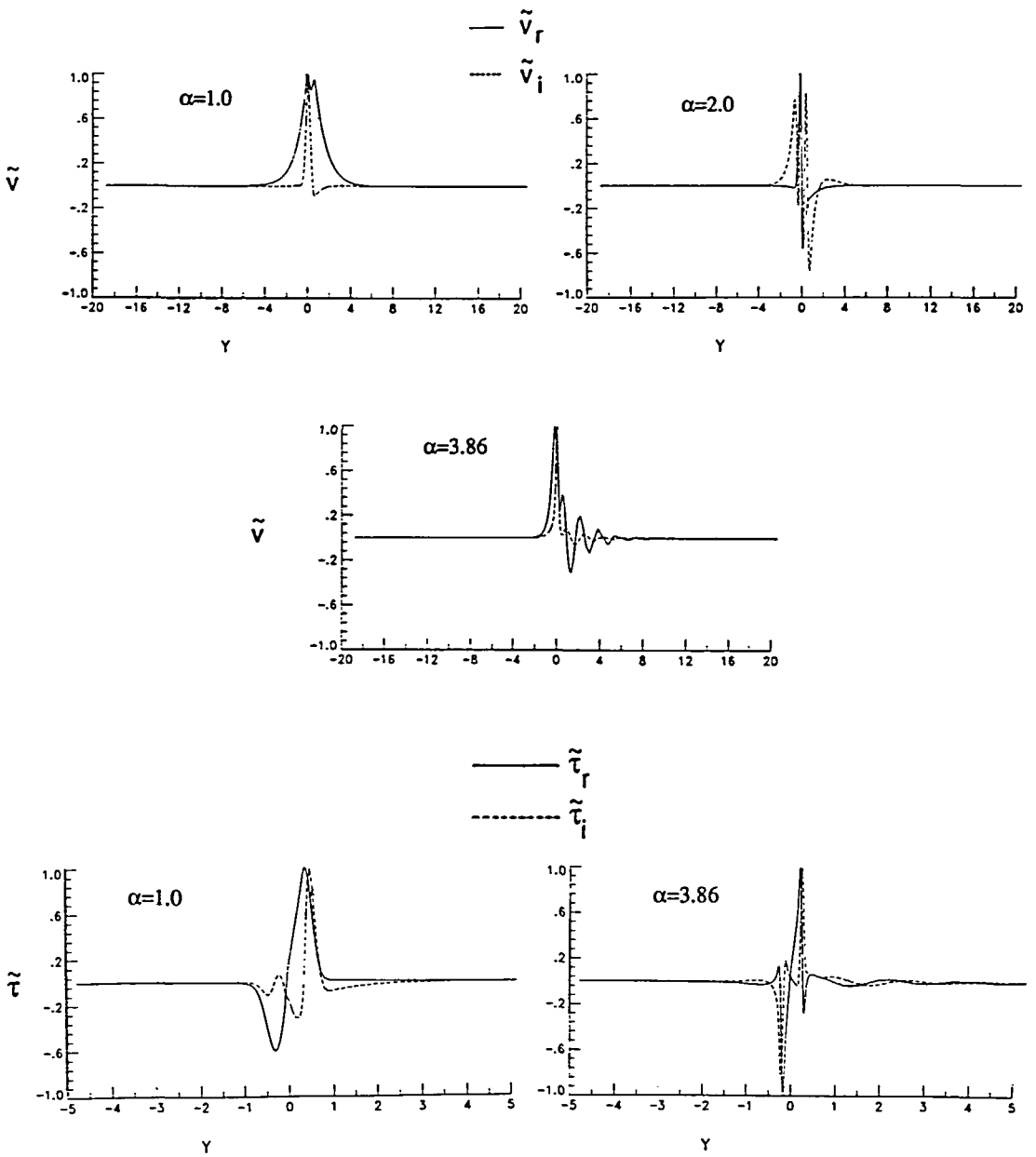

Figure 3 Velocity and temperature disturbance eigenfunctions for increasing α corresponding to station 1, Case I

SPATIAL SIMULATION

A spatial non-linear simulation is performed utilizing the spatially evolving mean flow described in the previous Section. The governing equations are the compressible Navier–Stokes equations written in Cartesian coordinates for two-dimensional flow. A Chebyshev spectral discretization is utilized in the normal direction, and a fourth-order compact difference scheme is used in the

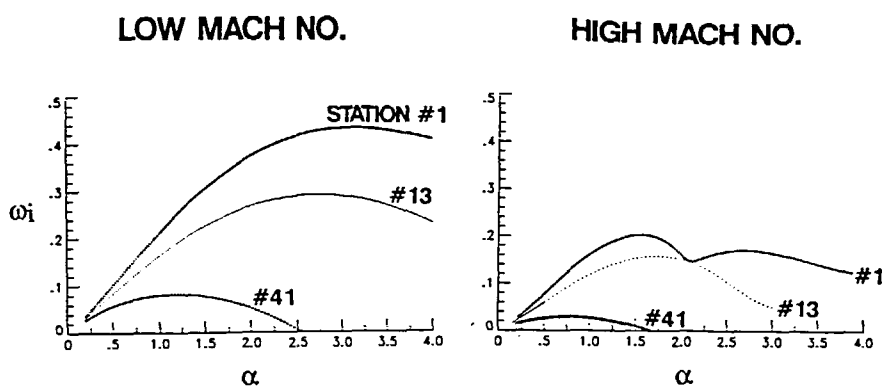

Figure 4 Temporal growth rates versus streamwise wavenumbers for mean flow stations of Case II: $M_1=0.6$, $M_2=0.4065$, $T_\infty=287.7$ K, $Re=50{,}000$, non-adiabatic. Case I is shown for comparison

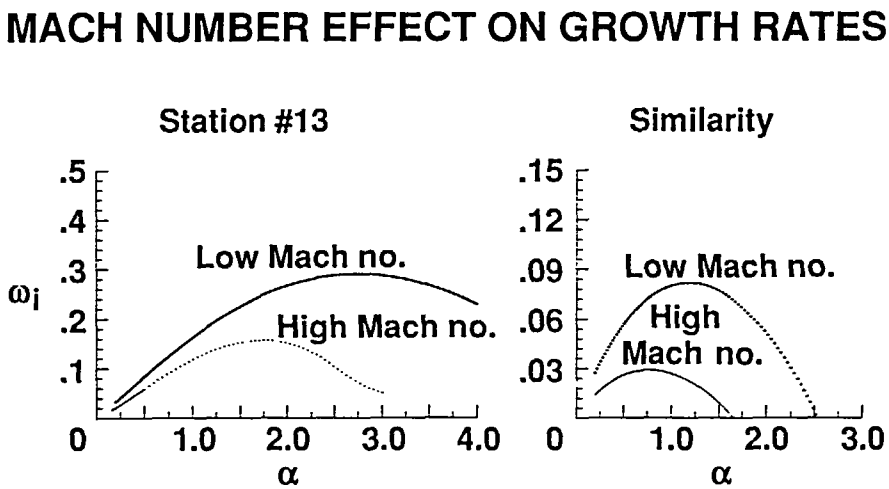

Figure 5 Plots of temporal growth rates versus α emphasizing the stronger effect of Mach number on maximum temporal growth rates for mean flow stations nearer the trailing edge of the splitter plate

streamwise direction. The time-stepping scheme is third-order and semi-implicit. A non-reflecting outflow boundary treatment is effected by appending a short 'buffer domain' to the end of the computational region, a technique developed by Streett[14]. In this region, typically only one or two primary wavelengths long, upstream reflections of disturbances from the outflow boundary are prevented through two modifications to the Navier–Stokes equations. First, the viscous terms responsible for streamwise-elliptic behaviour are multiplied by a smooth attenuation function which goes to zero at the outflow boundary. Second, to avoid upstream feedback due to the acoustic or pressure terms, the imposed base- or mean-flow is modified in the buffer domain so that the total streamwise velocity at the outflow boundary is supersonic. With all characteristics of the inviscid part of the equations outgoing at the boundary, therefore, the interior time-stepping scheme may be used to compute the solution at the boundary. At the inflow, the mean flow field plus harmonic disturbance is imposed throughout the spatial evolution.

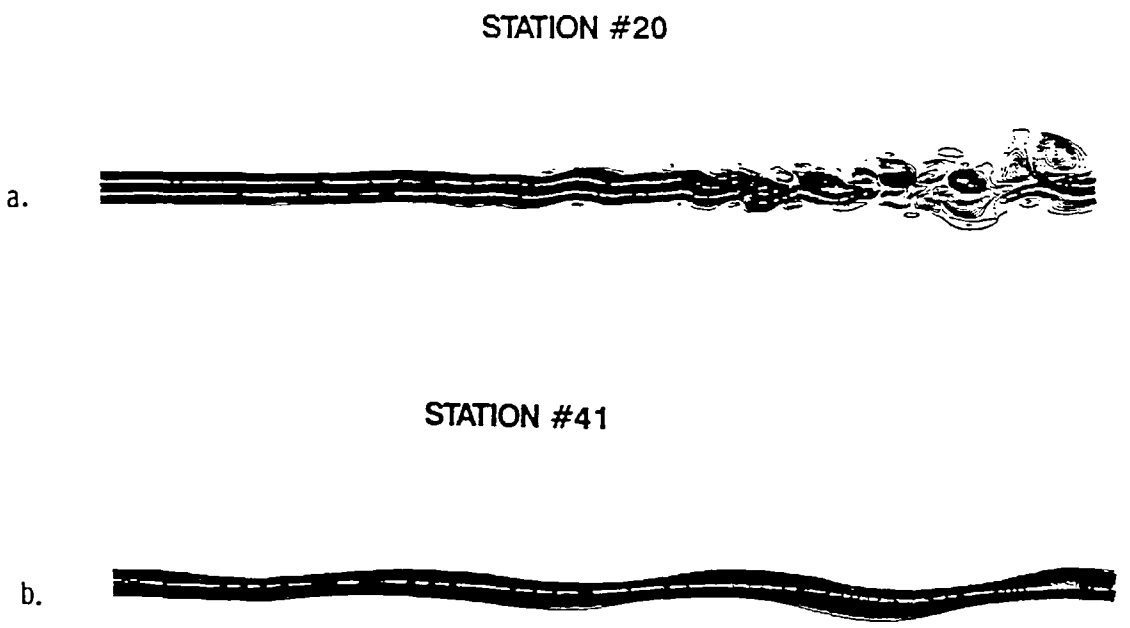

Figure 6 Total vorticity contours from spatial simulations for case I. (a) Station 20 utilized as the mean flow. (b) Similarity shear layer profile (station 41) utilized as the mean flow.

Two spatial simulations are presented. Maximally-unstable disturbances from stations 20 and 41 (near similarity) in case I are used as initial conditions along with the mean flow profiles from these stations, respectively. A 2% amplitude is imposed on the linear dusturbance in both cases. *Figure 6a* and *6b* depict total vorticity contours from station 20 and station 41, respectively. The simulation has progressed roughly 8 wavelengths downstream. A very strong roll up occurs if station 20 is used as the mean flow as depicted in *Figure 6a*. However, no vortex pairing and roll up is obtained when station 41 is utilized for the mean flow (*Figure 6b*).

CONCLUSIONS

A study of the linear and non-linear evolution of a spatially evolving wake is presented. The appearance of a higher mode for near wake profiles is seen when the free stream Mach numbers are supersonic. Downstream of the splitter plate, growth rates weaken, and this higher mode stabilizes before the flow asymptotes to an essentially similar profile. Contrasted with this supersonic flow are evolving wake profiles with subsonic free stream Mach numbers. It is found that the decrease in growth rate with increasing Mach number is much less for non-similar mean flows near the trailing edge. The non-linear spatial evolution of the supersonic wake exhibits a strong roll-up for the highly unstable near wake-region profiles. However, as similarity is approached further downstream of the splitter plate, no roll-up is obtained for this high Mach number flow.

ACKNOWLEDGEMENT

Special thanks is given to Dr C. L. Streett for providing the outflow buffer domain technique utilized in the simulations.

REFERENCES

1 Gropengiesser, H. *NASA TTF-12*, 786 (1969)
2 Jackson, T. and Grosch, C. *J. Fluid Mech.*, **208**, 208–683 (1989)
3 Macaraeg, M. and Streett, C. *Appl. Num. Math.*, **7**, 93–127 (1991)
4 Papamoschou, D. and Roshko, A. *AIAA Paper 86-0162* (1986)
5 Chen, J., Cantwell, B. and Mansour, N. *Phys. Fluids* (*A*), **II**, 984–1004 (1990)
6 Sandham, N. and Reynolds, W. *Turbulent Shear Flows*, Vol. 6, Springer-Verlag, Berlin, pp. 441–453 (1989)
7 Bushnell, D., personal communication (1990)
8 Pruett, D. and Streett, C. *J. Comput. Phys.*, in press (1991)
9 Macaraeg, M., Streett, C. and Hussaini, M. *NASA TP 2858* (1988)
10 Papageorgiou, D. and Smith, F. *Proc. R. Soc.* (*A*) **419**, 1–28 (1988)
11 Demetriades, A. and Brower, T. *AIAA 90-0710* (1990)
12 Papageorgious, D., *ICASE Report No. 90-39* (1990)
13 Zhuang, M., Kubota, T. and Dimotakis, P. *Proc. Ist Nat. Congr. Fluid Dynamics*, pp. 768–773 (1988)
14 Streett, C. and Macaraeg, M. *Appl. Num. Math.*, **2**, 123–139 (1986)